

Inhibiting flow-accelerated copper corrosion under liquid jet impingement by utilizing nanobubbles

Katagiri, Naruhito

Research and Development Headquarters, Rinnai Corporation

Kioka, Arata

Department of Earth Resources Engineering, Kyushu University

Nonoyama, Masao

Research and Development Headquarters, Rinnai Corporation

Hayashi, Yuichi

Research and Development Headquarters, Rinnai Corporation

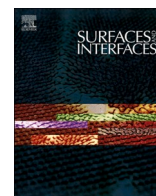
<https://hdl.handle.net/2324/6794436>

出版情報 : Surfaces and Interfaces. 40, pp.103067-, 2023-08. Elsevier

バージョン :

権利関係 : © 2023 The Authors.





Inhibiting flow-accelerated copper corrosion under liquid jet impingement by utilizing nanobubbles

Naruhito Katagiri^{a,*}, Arata Kioka^{b,*}, Masao Nonoyama^a, Yuichi Hayashi^a

^a Research and Development Headquarters, Rinnai Corporation, Aichi 480-0133, Japan

^b Department of Earth Resources Engineering, Kyushu University, Fukuoka 819-0395, Japan

ARTICLE INFO

Keywords:

Copper corrosion
Corrosion inhibition
Jet impingement
Nanobubbles
Ultrafine bubbles

ABSTRACT

Flow-accelerated corrosion can be very destructive, leading to rapid loss of component efficiency and eventual failure of the system; however, finding inexpensive, effective, and chemically benign inhibitors is still challenging. This paper studied for the first time the use of nanobubbles/ultrafine bubbles as a “green” functional nanostructured material for inhibiting flow-accelerated corrosion under the impingement of a turbulent liquid jet. We examined the corrosion inhibition of the copper specimen for 5 h in the flow regime at a Reynolds number of from 6.1×10^3 to 3.0×10^4 , with adding $\sim 6 \times 10^7$ bubbles/mL of air-nanobubbles to the tested liquid of 0.25% CuCl₂ solution at 40 °C. We measured weight losses, analyzed microstructure using SEM, and acquired maximum erosion depths and roughness curves of tested copper specimens. We found that nanobubbles mitigated flow-accelerated corrosion under jet impingement. The inhibition effectiveness was more significant at higher jet velocity and longer test time, with up to $43.9 \pm 0.1\%$ and $69.5 \pm 1.8\%$ based on weight losses and erosion depths, respectively. Nanobubbles play a role in reducing wall shear stress on the copper surface, likely by generating bubble mattresses. We suggest that nanobubbles inhibit the corrosion in highly erosive/corrosive turbulent conditions where most inhibitors could not work well.

1. Introduction

Copper, one of the essential nonferrous materials, is widely used in the equipment of broad industrial fields because of its noble physical properties and mechanical workability. Copper essentially represents good resistance to corrosion due to the formation of a passive protective film or nonconductive layer of corrosion products on its surface [1]. However, copper is susceptible to corrosion in several environmental conditions where oxygen or other oxidants are present, often leading to performance reduction in power plants, heat exchangers, cooling towers, shipbuilding, pipelines, electronics, and seawater desalination. The corrosion of copper pipes can also lead to increased copper concentration in drinking water that exceeds health guidelines [2]. Many studies have thus reported to understand the mechanism of copper corrosion and find new effective inhibitors of copper corrosion [1,3,4]. The inhibitors of copper corrosion reported in the earlier studies include azoles derivatives such as benzotriazole, thiazole, thiadiazole, and imidazole [5–8], Schiff bases [9,10], amino acids [11–14], self-assembled compounds [15,16], and “green” inhibitors such as natural inhibitors and pharmaceutical compounds [17,18]. Green corrosion

inhibitors are among the most demanded inhibitors because they are environmental-friendly; however, they generally provide a low efficiency of copper corrosion inhibition [1]. Advanced green nanostructured materials will modify the copper surface or change the physicochemical phenomena at the surface and interface of copper to achieve a high inhibition efficiency of copper corrosion.

Flow-accelerated corrosion is the corrosion resulting from the turbulence of fluid flow. Flow accelerates corrosion through the magnitude of fluid turbulence and the fluctuations in turbulence that occur in a liquid phase contacting the metal surface. The fluid flow itself has a role in flow-accelerated corrosion and erosion-corrosion by increasing the velocity of fluid impinging onto the metal surface and the mass transport rate of corrosive species to the surface. The corrosion rate increases with an increase in the surface roughness of a metal surface, and the influence of surface roughness is more pronounced under turbulent flow rather than laminar flow [19]. The flow-accelerated corrosion of copper is facilitated in the presence of greater surface roughness [4], and thus reducing surface roughness is essential to mitigate copper corrosion. In jet impingement tests, many studies investigated the mechanisms of corrosion mitigation in the presence of tens of micromillimeter-thick

* Corresponding authors.

E-mail addresses: naruhitokatagiri@rinnai.co.jp (N. Katagiri), kioka@mine.kyushu-u.ac.jp (A. Kioka).

<https://doi.org/10.1016/j.surfin.2023.103067>

Received 18 April 2023; Received in revised form 10 June 2023; Accepted 12 June 2023

Available online 14 June 2023

2468-0230/© 2023 The Authors. Published by Elsevier B.V. This is an open access article under the CC BY license (<http://creativecommons.org/licenses/by/4.0/>).

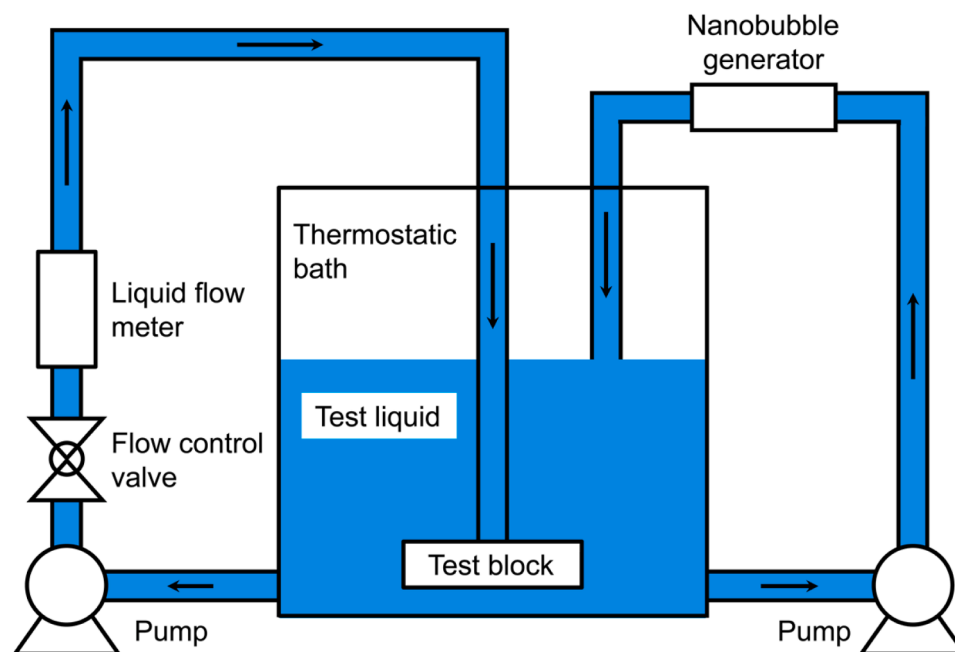


Fig. 1. Schematic illustration of jet impingement test apparatus. See Fig. 2 for the detail of test block.

films [20] and the erosion processes due to liquid flow laden with nanoparticles such as TiO_2 [21]. Metal nanoparticles can be colloidal additives to reduce friction and improve antiwear. In turbulent flow conditions, one of the most effective ways to mitigate corrosion is reducing the Reynolds stresses (wall shear stresses) on the metal surface [22]. A few green inhibitors can inhibit aluminum-alloy corrosion under jet impingement with a maximum inhibition efficiency of 58% [23,24]. However, to our knowledge, no previous green inhibitors for copper corrosion are effective in turbulent flow conditions because most green inhibitors cannot withstand high shearing conditions.

Nanobubbles (NBs) or ultrafine bubbles are tiny bubbles with a typical diameter of 50–200 nm and a height above the substrate of a few tens of nm [25–28]. NBs are a growing discipline that has advanced understanding of their physicochemical properties and broadened their applications in many fields [28–31]. Longevity of several weeks to several months and stability due to pinning on the solid surface are among the most valuable characteristics of NBs [32–34]. When NBs are pinned on the surface of a solid substrate, the surface NBs represent unique physicochemical characteristics at the interface between a liquid medium and a solid substrate. NBs are also stable with respect to

increases in temperature and pressure [35,36]. NBs can be generated by many types of gasses, including air, H_2 , N_2 , O_2 , CO_2 , and O_3 , as per the interest in the physicochemical properties of NBs. NBs are valuable for surface nanoscopic materials in the context of numerous modern applications germane to the interactions of surfaces and interfaces. Thus, many studies have worked for utilizing NBs as a green solution, including controls of crystal growth and morphology [37–40], manipulations of nanoparticles and cells [41,42,43], drug delivery [44,45], wastewater treatments [31], enhanced bacterial growth [46], plant growth [47], food processing [48], and mineral flotation [49–51]. A few studies recently suggested that NBs can help mitigate corrosion in geo-fluid [52,53]. These studies found the effectiveness of corrosion inhibition for mild-carbon steel in an acidic medium at high temperatures. However, all the previous publications only studied corrosion inhibition in a no-flow condition or a condition with very slow fluid flows. Therefore, no papers to our best knowledge have investigated whether NBs can mitigate corrosion of the metal subject to fluid flow with a high velocity. This paper is the first study presenting that NBs can inhibit corrosion in highly erosive/corrosive and turbulent conditions where most inhibitors cannot work well. This paper also discusses how NBs

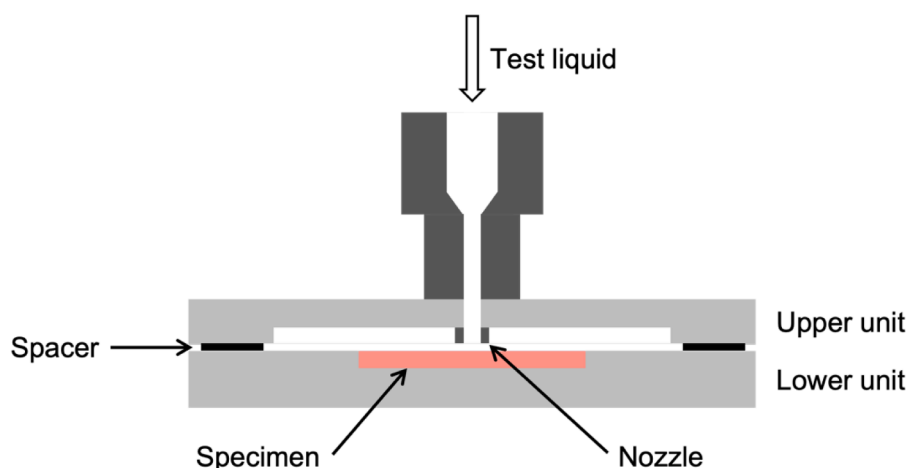


Fig. 2. Test block of jet impingement test.

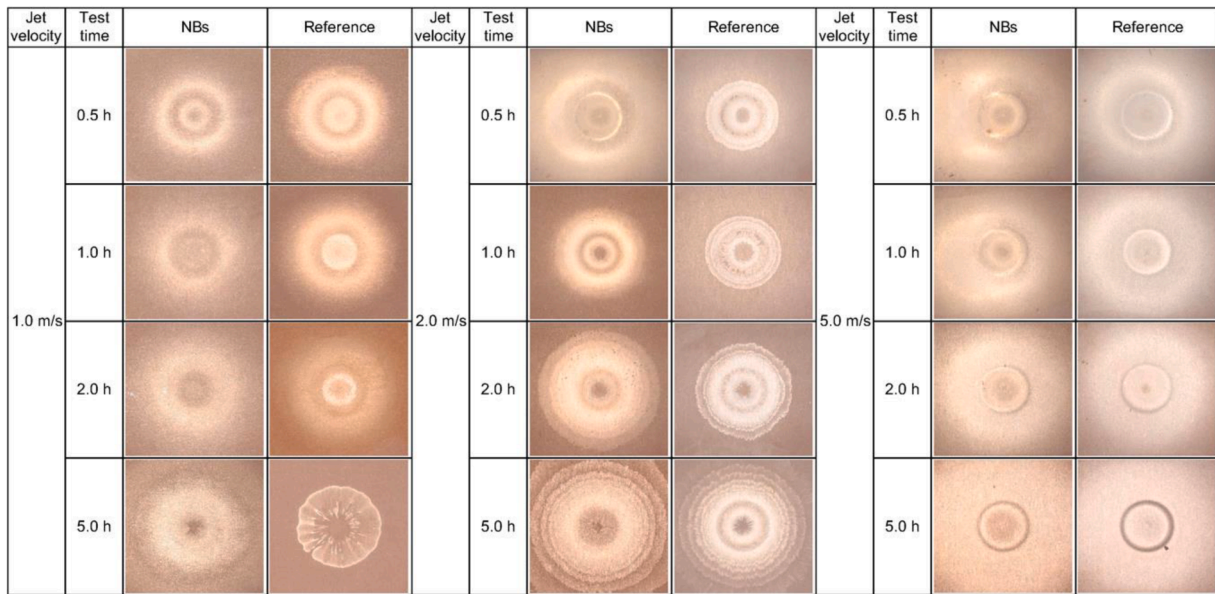


Fig. 3. Photos of specimens after 0.5, 1.0, 2.0, and 5.0 h of jet impingement test at jet exit velocities of 1.0, 2.0, and 5.0 m/s with the NBs-containing CuCl_2 and reference CuCl_2 solutions. The width of photo of given specimen is 30 mm.

influence the surface of studied corrosive material leading to corrosion mitigation.

2. Methods and materials

The test apparatus of jet impingement consists of a thermostatic bath to maintain the temperature of the test solution (8 L) at a constant level, a pump to deliver the solution to the test stand, and a flow meter (Fig. 1). The copper specimen was placed at the bottom of the test stand with a 1.0 mm gap between the 4.0 mm diameter jet nozzles and the surface of the copper specimen (Fig. 2). The jet flowed directly into the center of the specimen. The confined jet involved the injection of test liquid into a confined space above the surface of the copper specimen. The confinement wall was parallel to the surface of the copper specimen. The height-to-diameter ratio was 0.25. When the NBs-containing solution flowed in the jet impingement test, we added a NB generator and a pump for pumping liquid to the NB generator in the test apparatus. NBs were generated using a shear-type NB generator (Rinnai Corp., Japan, mounted on RUF-UE2406AW). This NB generator uses dissolved oxygen in the liquid to generate air-NBs without introducing external gas. The gas-supersaturated liquid is expelled through a nozzle and depressurized, leading to gasify the dissolved air and nucleate fragmented air-NBs. The size and number density of generated NBs in the 8 L solution were analyzed using a NanoSight NS300 (Malvern Panalytical Ltd., UK). The median diameter of generated NBs was 75 ± 5 nm at the studied temperature of 40°C . The number density of NBs increased linearly with the operating time of the generator in the first ~ 10 min, from 2×10^7 to 6×10^7 bubbles/mL. The number density reached saturation after 10 min of operation, and it was $6.0(\pm 0.4) \times 10^7$ bubbles/mL between 10 and 30 min. Based on these results, when performing the jet impingement test with the NBs-containing liquid, we started generating NBs by operating the NB generator for 30 min before conducting the test. We generated NBs continuously throughout the test.

The test material was phosphorus-deoxidized copper (JIS H 3100 standard). Its chemical composition is $\text{Cu} \geq 99.90\%$ and $\text{P} 0.015\text{--}0.040\%$. The rectangular specimens with dimension of $30 \times 40 \times 3$ mm (width \times length \times thickness) were prepared, and the copper specimen surfaces were wet-polished to #2000 with water-resistant polishing paper. The weight of the copper specimen before the jet impingement test was about 32 g. The specimens were then degreased,

acid-washed with 10% H_2SO_4 , and acetone-substituted for testing. Eight liters of 0.25% CuCl_2 (II) solution were used as the accelerated test solution, and the temperature of the test solution was 40°C . The flow rate was adjusted in the range of 0.75–3.77 L/min so that the flow velocities at the nozzle outlet (jet exit velocities) were 1.0, 2.0, and 5.0 m/s in order to investigate the effect of flow velocity. Test durations were 0.5, 1.0, 2.0, and 5.0 h to monitor the progress of corrosion. After the test, the specimens were cleaned by ultrasonic cleaning to remove corrosion products on the surface, degreased, acid cleaned, and replaced with acetone before evaluation.

A higher jet exit velocity at the nozzle outlet results in the reduction of corrosion resistance of the tested material. The Reynolds number is defined as:

$$Re = \frac{2r_0u_0}{\nu}, \quad (1)$$

where r_0 is the inner radius of the jet nozzle, u_0 is the flow velocity at the nozzle outlet, and ν is the kinematic viscosity of the studied solution ($0.66 \text{ mm}^2/\text{s}$ at 40°C). Reynolds numbers at the flow velocities of 1.0 m/s and 5.0 m/s were 6.1×10^3 and 3.0×10^4 , respectively. The critical Reynolds number Re_c at the laminar-turbulent transition for the single impinging jet flow is 2×10^3 [54], indicating that the flow regime in our experiment is turbulent. In the turbulence region, the wall shear stress τ_w (N/m^2) is calculated by:

$$\tau_w = 0.179\rho u_0^2 Re^{-0.182} (r/r_0)^{-2}, \quad (2)$$

where ρ is the density of the studied fluid ($992 \text{ kg}/\text{m}^3$ at 40°C), and r is the radial distance from the center of the specimen [55–57]. In our experiment with the flow velocities at the nozzle outlet of 1.0 m/s and 5.0 m/s, the wall shear stresses τ_w at $r/r_0 = 3$ in the high turbulence region were 4.0 and 75 Pa, respectively.

We sampled the specimens from the reference solution and NBs-containing solution after 0.5, 1.0, 2.0, and 5.0 h of the jet impingement test. The post-test specimens were evaluated by visual observation, microstructure observation, corrosional weight loss, maximum erosion depth, and linear roughness curve. The external appearance was observed using a Keyence VHX-6000 digital microscope. The surface microstructure of the specimen was observed using a JEOL JSM-IT700HR scanning electron microscope (SEM). The corrosion loss Δm

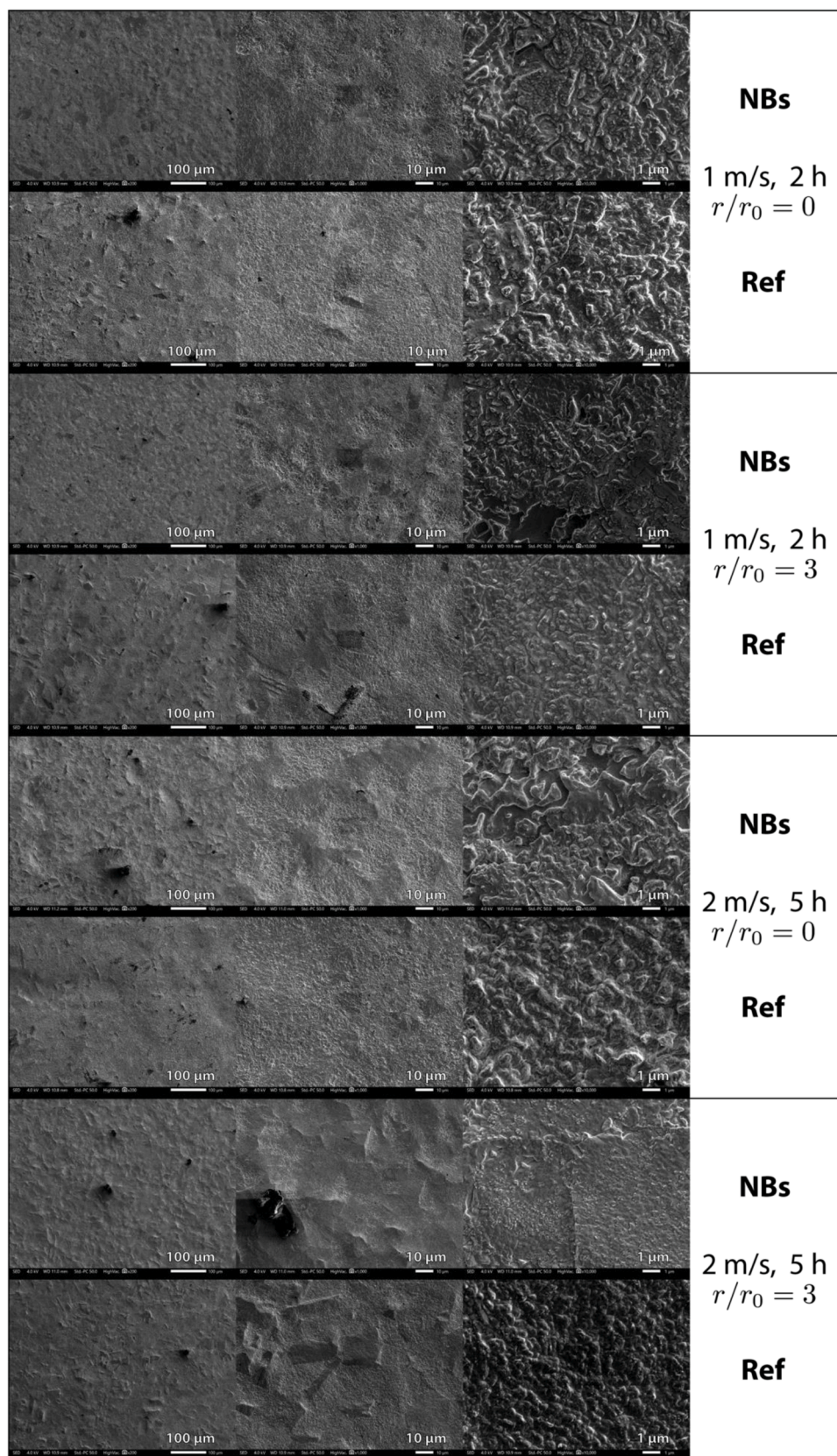


Fig. 4. SEM images at the center of specimen ($r/r_0 \sim 0$) and ~ 6 mm from the center of given specimen ($r/r_0 \sim 3$) with the reference CuCl_2 solution (“Ref”) and NBs-containing CuCl_2 solution (“NBs”).

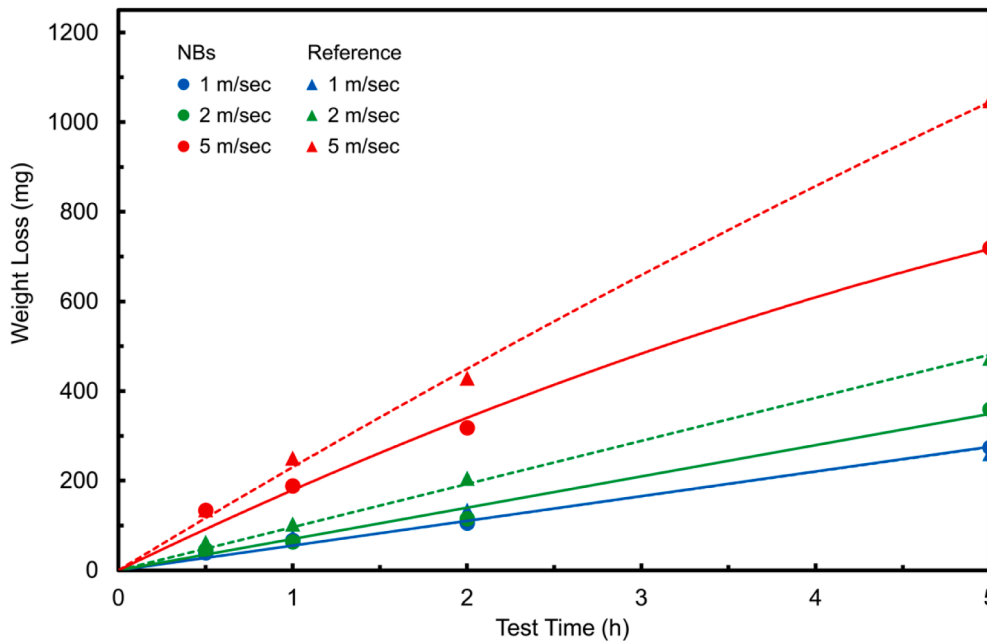


Fig. 5. Weight loss of the given specimen from the reference CuCl_2 solution and NBS-containing CuCl_2 solution after jet impingement test for 0.5, 1.0, 2.0, and 5.0 h with a jet exit velocity of 1.0, 2.0, and 5.0 m/s.

(± 0.1 mg) was calculated from the weight of the specimens before and after the test. The maximum erosion depth z_{\max} and line roughness curve $z(r)$ were measured using a Keyence VR-3200 wide-area 3D measurement system. The maximum erosion depth was produced using surface roughness analysis (ISO 25,128 standard). The roughness curve was acquired by line roughness analysis (JIS B 0601 standard) in the longitudinal direction of the specimen passing through the center of the given specimen. The vertical accuracy was $\pm 3 \mu\text{m}$. We acquired the roughness curve of the specimens that had significant differences between the weight losses in the reference CuCl_2 fluid and NBS-containing CuCl_2 fluid. We also computed the arithmetic average surface roughness R_a from the obtained roughness profiles.

We evaluated the inhibition efficiency (%) by obtaining three different inhibition efficiency indices based on the weight loss ($\eta_{WL}(t)$), the maximum erosion depth from 3D surface roughness analysis ($\eta_{MD}(t)$), and the roughness curve from line roughness analysis ($\eta_{RC}(r, t)$). The three inhibition efficiencies at t (h) were calculated by:

$$\eta_{WL}(t) = (\Delta m_{\text{ref}}(t) - \Delta m_{\text{NB}}(t)) / \Delta m_{\text{ref}}(t) \times 100, \quad (3)$$

$$\eta_{MD}(t) = (z_{\max, \text{ref}}(t) - z_{\max, \text{NB}}(t)) / z_{\max, \text{ref}}(t) \times 100, \quad (4)$$

$$\eta_{RC}(r, t) = (z_{\text{ref}}(r, t) - z_{\text{NB}}(r, t)) / z_{\text{NB}}(r, t) \times 100, \quad (5)$$

where $\Delta m_{\text{ref}}(t)$ (mg) and $\Delta m_{\text{NB}}(t)$ (mg) are the weight losses of the specimens after t (h) of jet impingement test with the reference CuCl_2 solution and NBS-containing CuCl_2 solution, $z_{\max, \text{ref}}(t)$ and $z_{\max, \text{NB}}(t)$ are the maximum erosion depths of the specimens in the reference CuCl_2 fluid and the NBS-containing CuCl_2 fluid at t (h), and $z_{\text{ref}}(r, t)$ and $z_{\text{NB}}(r, t)$ are the depths of the specimens at the radial distance r (μm) in the reference CuCl_2 fluid and the NBS-containing CuCl_2 fluid at t (h), respectively. Smaller weight loss $\Delta m_{\text{NB}}(t)$ and erosion depths $z_{\max, \text{NB}}(t)$ and $z_{\text{NB}}(r, t)$ of the specimen in the NBS-containing fluid yield better inhibition efficiencies of $\eta_{WL}(t)$, $\eta_{MD}(t)$ and $\eta_{RC}(r, t)$ by NBS at a given time t (h).

3. Results

3.1. Visual inspection and surface microstructure of tested specimens

The specimens were sampled from the reference CuCl_2 solution and the NBS-containing CuCl_2 solution after 0.5, 1.0, 2.0, and 5.0 h of the jet impingement test with jet exit velocities of 1.0, 2.0, and 5.0 m/s. From the photographs of the surfaces of tested specimens taken using a digital microscope (Fig. 3), we found ring-shaped depressions on the surfaces of all the tested specimens at 5–6 mm from the center of the specimen ($2.5 < r/r_0 < 3$). We also identified noticeable visual differences between the specimens at all the test time and jet exit velocities with the reference CuCl_2 solution and the NBS-containing CuCl_2 solution. Interestingly, the erosion corrosion in the NBS-containing CuCl_2 solution generally radiated broader than that in the reference CuCl_2 solution when a jet exit velocity was 1.0 m/s and 2.0 m/s. However, it was not found when the jet exit velocity was 5.0 m/s (Fig. 3).

We obtained SEM images of the tested specimen at the center of the given specimen ($r/r_0 \sim 0$) and ~ 6 mm from the center of the given specimen ($r/r_0 \sim 3$) with magnifications of $\times 200$, $\times 1000$ and $\times 10,000$ (Fig. 4). As expected from visual inspections of specimens, SEM images generally showed that the surfaces were more eroded when the test time of jet impingement was longer and jet exit velocity was higher. We also identified a few small holes and grooves from the specimens. However, we did not find significant differences between the tested specimens from the reference CuCl_2 solution and the NBS-containing CuCl_2 solution at any test time and jet exit velocity.

3.2. Weight losses and maximum erosion depths of tested specimens

Weight losses of the specimens were prominent with a longer time of jet impingement test and higher jet exit velocity (Fig. 5). The weight loss increased linearly with time, and it was 134.9 mg (0.42% of the pre-test weight), 250.5 mg (0.79%), 429.0 mg (1.35%), and 1047.5 mg (3.29%) after 0.5, 1.0, 2.0, and 5.0 h, respectively, of jet impingement test with the reference CuCl_2 solution and a jet exit velocity of 5 m/s. We found the weight losses of the specimen with the NBS-containing CuCl_2 solution after 0.5, 1.0, 2.0, and 5.0 h of jet impingement test with all the cases of jet exit velocity were generally smaller than those with the

Table 1Inhibition efficiencies of $\eta_{WL}(t)$ and $\eta_{MD}(t)$ at a given time t (h).

Inhibition efficiency	Jet exit velocity	Test time of jet impingement (t)			
		0.5 h	1.0 h	2.0 h	5.0 h
$\eta_{WL}(t)$	2.0 m/s	27.6 \pm 0.3%	38.3 \pm 0.2%	43.9 \pm 0.1%	24.1 \pm 0.0%
	5.0 m/s	0.8 \pm 0.1%	24.7 \pm 0.1%	25.9 \pm 0.0%	31.3 \pm 0.0%
$\eta_{MD}(t)$	2.0 m/s	7.2(+7.7/−8.4)%	30.0(+3.6/−3.8)%	40.4(+3.0/−3.2)%	35.5 \pm 2.5%
	5.0 m/s	39.6(+3.9/−4.1)%	69.5 \pm 1.8%	67.1 \pm 1.8%	60.2 \pm 1.5%

reference CuCl_2 solution after the respective time of test (Fig. 5). This resulted in the weight-loss-based corrosion inhibition effectiveness $\eta_{WL}(t)$ of the tested specimens after 0.5, 1.0, 2.0, and 5.0 h of jet impingement with a jet exit velocity of 2 m/s was 28%, 38%, 44%, and 24%, respectively (Table 1). The weight-loss-based corrosion inhibition effectiveness $\eta_{WL}(t)$ after 5.0 h of jet impingement was better when a jet exit velocity was higher. The weight-loss-based corrosion inhibition effectiveness $\eta_{WL}(t)$ increased with test time when a jet exit velocity was 5.0 m/s. In contrast, the jet impingement with the lowest jet velocity of 1.0 m/s did not achieve good weight-loss-based inhibition effectiveness $\eta_{WL}(t)$, falling within 0% to 21%.

Maximum erosion depths of the specimens were greater with a longer time of jet impingement test and higher jet exit velocity (Fig. 6). The maximum erosion depth increased logarithmically with time, and it was 122 ± 3 μm , 216 ± 3 μm , 221 ± 3 μm , and 280 ± 3 μm after 0.5, 1.0, 2.0, and 5.0 h, respectively, of jet impingement test with the reference CuCl_2 solution and a jet exit velocity of 5.0 m/s. As we found in the weight losses of specimens, maximum erosion depths of specimens with the NBs-containing CuCl_2 solution after 0.5, 1.0, 2.0, and 5.0 h of jet impingement test were generally less than those with the reference CuCl_2 solution after the respective time of test (Fig. 6). Notably, the reduction in maximum erosion depth was generally more significant when a jet exit velocity was higher. The corrosion inhibition effectiveness based on maximum erosion depth $\eta_{MD}(t)$ of the tested specimens after 0.5, 1.0, 2.0, and 5.0 h of jet impingement with a jet exit velocity of 5.0 m/s was $40 \pm 4\%$, $70 \pm 2\%$, $67 \pm 2\%$, and $60 \pm 2\%$, respectively (Table 1). The corrosion inhibition effectiveness based on maximum erosion depth $\eta_{MD}(t)$ after 5.0 h of jet impingement increased from nearly zero to 60% with a jet exit velocity increase from 1.0 to 5.0 m/s. The effectiveness of corrosion inhibition based on maximum erosion

depth $\eta_{MD}(t)$ was greater than that based on weight loss $\eta_{WL}(t)$ when a jet exit velocity was 5.0 m/s. In contrast, the result after 0.5, 1.0, and 2.0 h was the opposite when a jet exit velocity was 2.0 m/s. As expected from the weight loss result, the corrosion inhibition effectiveness based on maximum erosion depth with the lowest jet velocity of 1.0 m/s was low, ranging from 0% to 29%.

3.3. Roughness curve of specimens

We obtained the roughness curve of the given specimen in the longitudinal direction passing through the center of the given specimen. Two depressions were identified at the position of $0 \leq r/r_0 \leq 2$ and $2 < r/r_0 \leq 4$ of the given specimen tested for 0.5, 1.0, 2.0, and 5.0 h. When a jet exit velocity was 2.0 m/s, the roughness curves showed that the erosion of the specimen with NBs-containing CuCl_2 solution was mitigated more than that with the reference CuCl_2 solution (Fig. 7a). For example, the height profile of the specimen with NBs-containing CuCl_2 solution after 1.0 h of jet impingement was almost identical to that with the reference CuCl_2 solution after a shorter time of 0.5 h of jet impingement. The NBs-containing CuCl_2 solution generally showed corrosion inhibition throughout the specimen surface (Fig. 7b). The inhibition efficiency was generally greater with a longer test time, except for a test time of 2.0 h which was not successful for inhibition at the radial distance of $r/r_0 > 4$. At the radial distance of $r/r_0 > 4$, the arithmetic average surface roughness R_a with a jet exit velocity of 2.0 m/s did not show significant differences between the reference CuCl_2 solution and NBs-containing CuCl_2 solution after 0.5, 1.0, and 2.0 h of jet impingement test (Fig. 8). However, changes in arithmetic average surface roughness R_a at the radial distance of $0 \leq r/r_0 \leq 4$ were quite contrasting. The arithmetic average surface roughness R_a at the radial distance of $0 \leq r/r_0 \leq 4$ with

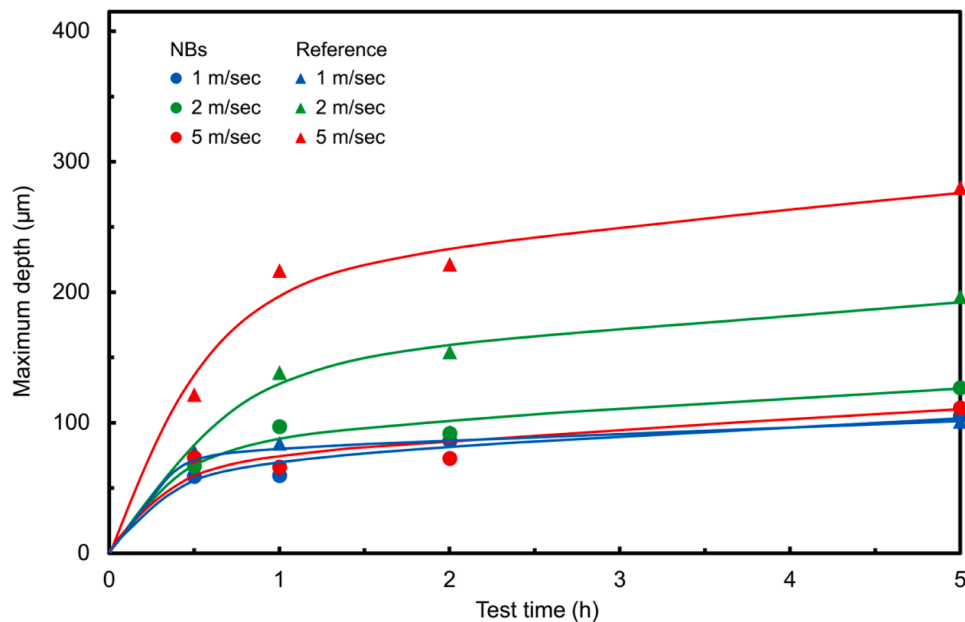


Fig. 6. Maximum erosion depth of the give specimen from the reference CuCl_2 solution and NBs-containing CuCl_2 solution after jet impingement test for 0.5, 1.0, 2.0, and 5.0 h with a jet exit velocity of 1.0, 2.0, and 5.0 m/s. The accuracy of measured maximum erosion depth is ± 3 μm .

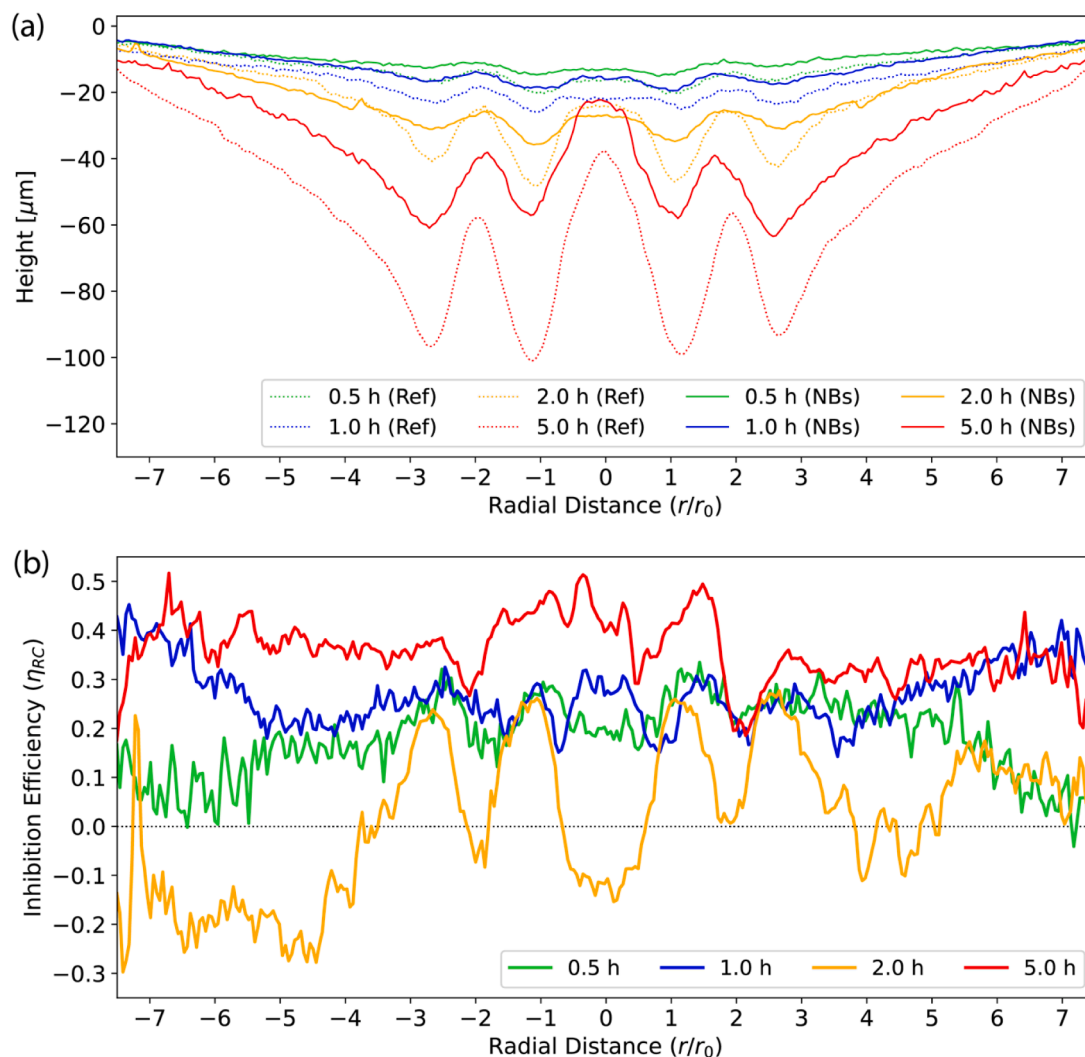


Fig. 7. (a) Surface roughness of the given specimen with the reference CuCl_2 solution (“Ref”) and NBs-containing CuCl_2 solution (“NBs”) after jet impingement test for 0.5, 1.0, 2.0, and 5.0 h with a jet exit velocity of 2.0 m/s. The accuracy of measured height is $\pm 3 \mu\text{m}$. (b) Inhibition efficiency $\eta_{RC}(r, t)$ at 0.5, 1.0, 2.0, and 5.0 h of jet impingement test with a jet exit velocity of 2.0 m/s.

the reference CuCl_2 solution increased linearly with test time, while the NBs-containing CuCl_2 solution retarded the increase after 5.0 h of the test. This resulted in that the average of the inhibition efficiency based on the roughness curve $\overline{\eta_{RC}}(r, t)$ after 5.0 h of test with a jet exit velocity of 2 m/s was 41%, 32%, and 35% at the position of $0 \leq r/r_0 \leq 2$, $2 < r/r_0 \leq 4$, and $4 < r/r_0 \leq 6$, respectively (Table 2), which were identical to the inhibition effectiveness based on maximum erosion depth $\eta_{MD}(t)$.

When a jet exit velocity was 5.0 m/s, the radial distance of $2 < r/r_0 \leq 4$ had the most profound depression in the specimen surface of 1.0, 2.0, and 5.0 h of jet impingement (Fig. 9a). The erosion of the specimen with NBs-containing CuCl_2 solution was generally less than that with the reference CuCl_2 solution when a jet exit velocity was 5.0 m/s. The inhibition efficiency $\eta_{RC}(r, t)$ was better with a longer test time (Fig. 9b). The height profile and arithmetic average surface roughness R_a throughout the specimen with NBs-containing CuCl_2 solution after 2.0 h of jet impingement were almost identical to those with the reference CuCl_2 solution after a shorter time of 1.0 h of jet impingement (Figs. 9a and 10). The increased rate of arithmetic average surface roughness R_a from 2.0 to 5.0 h was higher than that from 1.0 to 2.0 h with the two solutions when a jet exit velocity was 5.0 m/s (Fig. 10). However, the increase rate of arithmetic average surface roughness R_a with the reference CuCl_2 solution was higher than that with NBs-containing CuCl_2 solution throughout the surface of the given specimen. This

resulted in the NBs-containing CuCl_2 solution generally representing good inhibition throughout the surface of the specimen after 5.0 h of the test, with the averaged inhibition efficiency $\overline{\eta_{RC}}(r, t)$ of 41%, 42%, and 44% at the position of $0 \leq r/r_0 \leq 2$, $2 < r/r_0 \leq 4$, and $4 < r/r_0 \leq 6$, respectively (Table 2). However, the NBs-containing CuCl_2 solution did not pose a significant corrosion inhibition around the positions of the jet nozzle ($0 \leq r/r_0 \leq 0.5$).

4. Discussion

Recent two studies [52,53] suggested the effectiveness of corrosion inhibition by NBs for low-carbon steel in an acidic medium at high temperatures. However, these works only studied corrosion inhibition in a no-flow condition or a condition with very slow fluid flows. This paper examined, for the first to our best knowledge, whether NBs inhibit flow-accelerated corrosion under the impingement of a turbulent liquid jet based on weight losses, surface roughness profiles, and maximum erosion depths of tested specimens. We found that NBs prevented the copper specimens from corrosional erosion and weight loss throughout most of the specimen surface. Given these findings, we now anticipate that NBs can inhibit the corrosion of most of the metal compounds. Also, in our study, NBs exhibited good copper corrosion inhibition efficiencies even with a very high jet exit velocity of 5.0 m/s ($Re = 3.0 \times 10^4$),

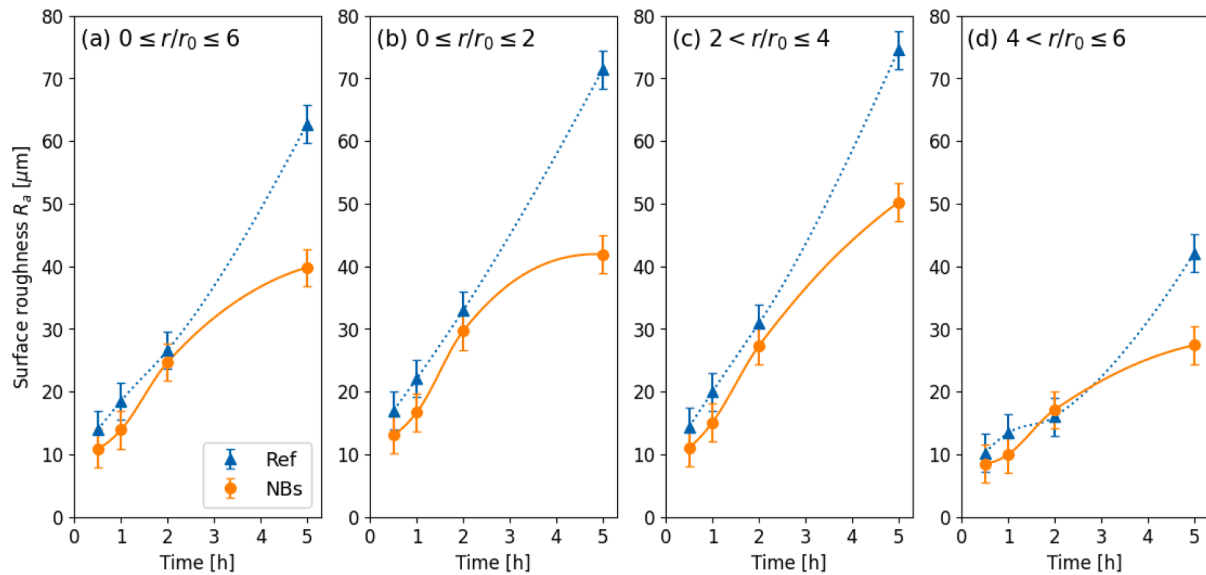


Fig. 8. Arithmetic average roughness R_a of the given specimen with the reference CuCl_2 solution (“Ref”) and NBs-containing CuCl_2 solution (“NBs”) after jet impingement test for 0.5, 1.0, 2.0, and 5.0 h with a jet exit velocity of 2.0 m/s. (a) Arithmetic average roughness R_a at the radial distance of $0 \leq r/r_0 \leq 6$. (b) Arithmetic average roughness R_a at the radial distance of $0 \leq r/r_0 \leq 2$. (c) Arithmetic average roughness R_a at the radial distance of $2 < r/r_0 \leq 4$. (d) Arithmetic average roughness R_a at the radial distance of $4 < r/r_0 \leq 6$.

Table 2

Average of the inhibition efficiency $\overline{\eta}_{RC}(r, t)$ at a given time t (h).

Jet exit velocity	Test time	$0 \leq r/r_0 \leq 2$	$2 < r/r_0 \leq 4$	$4 < r/r_0 \leq 6$
2.0 m/s	0.5 h	23.1%	22.9%	17.0%
	1.0 h	24.4%	23.8%	25.7%
	2.0 h	6.6%	9.6%	~0%
	5.0 h	40.9%	32.4%	35.1%
5.0 m/s	1.0 h	10.2%	19.1%	8.6%
	2.0 h	19.3%	28.3%	23.6%
	5.0 h	41.4%	42.2%	44.4%

resulting in $\eta_{WL}(t) = 31\%$, $\eta_{MD}(t) = 60 \pm 2\%$, and $\overline{\eta}_{RC}(r, t) = 43\%$ when the tested time of jet impingement was 5.0 h (Table 1 and Table 2). Moreover, the inhibition efficiencies were generally better with a longer time of jet impingement test within the tested period of 5.0 h (e.g., Figs. 7b and 9b). These findings suggest that the inhibition performance of NBs is well archived with higher jet exit velocities over a longer time than we studied. NBs can be an advanced green material to achieve high corrosion inhibition efficiencies by modifying the metal surface or changing the physicochemical properties at the surface and interface of the solid substrate.

Typical flow characteristics due to jet impingement on a flat substrate are well studied in earlier works [56]. The region at the radial distance $0 \leq r/r_0 \leq 2$ is the stagnation zone with a stagnation point at the center of the substrate. The flow is basically laminar near the plate and is accelerated to its maximum velocity at the radial distance of $r/r_0 = 2$. The region at the radial distance of $2 < r/r_0 \leq 4$ represents the flow of rapidly increasing turbulence with a high wall shear stress. In the region at $r/r_0 > 4$, the jet flow entrains more surrounding fluid, and its turbulence attenuates rapidly. Our results of the jet impingement test with both the reference CuCl_2 solution and NBs-containing CuCl_2 solution showed that the region at the radial distance of $2 < r/r_0 \leq 4$ was among the most eroded (Figs. 8–10). However, NBs presented good corrosion inhibition at the radial distance of $2 < r/r_0 \leq 4$, comparable to the corrosion inhibition at the radial distance of $0 \leq r/r_0 \leq 2$ and $4 < r/r_0 \leq 6$ (Table 2 and Figs. 7–10). These findings indicate that NBs inhibit flow-accelerated corrosion in both the laminar flow regime and the highly erosive/corrosive and turbulent conditions where most inhibitors

cannot work well.

NBs in our jet impingement test can be present in the bulk of the tested liquid solution and at the surface of the specimen. We cannot conclude which bulk NBs or surface NBs are the most significant player in mitigating flow-accelerated copper corrosion. However, recent studies suggest surface NBs can reduce the friction of liquid flow at the liquid-solid interface [58,59]. NBs can thus change the wettability and significantly increase the slip length at the interface. In turbulent flow conditions, reducing the Reynolds stresses (wall shear stresses) on the metal surface is essential to mitigate corrosion [22,60,61]. Below, we estimate the reduction in wall shear stress due to adding NBs to the solution in light of a well-known relationship between wall shear stress and corrosion rates. The wall shear stress τ_w (Pa) is defined as:

$$\tau_w = \mu \left(\frac{\partial u}{\partial y} \right)_{y=0} \quad (6)$$

where μ (Pa·s) is the dynamic viscosity, u (m/s) is the velocity of flow parallel to the specimen surface, and y (m) is the distance from the specimen surface. Here, we can approximate the change in wall shear stress due to adding NBs to the solution as the change in the flow velocity gradient (shear rate) near the surface $(\partial u / \partial y)_{y=0}$, given that the difference between the dynamic viscosities of the reference CuCl_2 solution and NBs-containing CuCl_2 solution is negligible. Efid et al. [56] provide a generalized equation representing the effect of wall shear stress on corrosion rates. It is expressed by the power law relationship between corrosion rate R_{corr} (mm/yr) and wall shear stress τ_w (Pa) at the given point of the metal surface:

$$R_{\text{corr}} = a \tau_w^b, \quad (7)$$

where a (mm/yr) and b are constants related to the specific environment and solution chemistry. Here, the wall shear stress τ_w increases nonlinearly with a higher jet exit velocity u_0 , as represented in Eq. (2). The wall shear stresses τ_w at $r/r_0 = 3.0$ for jet exit velocities of 1.0, 2.0, and 5.0 m/s are calculated as 4.0, 14, and 75 Pa, respectively, from Eq. (2). By determining the nonlinear least-squares estimates of the constants of the model Eq. (7), we can obtain $a = 47.2 \pm 9.3$ (mm/yr) and $b = 0.402 \pm 0.050$ from our results of the jet impingement test with the reference solution at 5.0 h, $r/r_0 = 3.0$, and jet exit velocities of 1.0, 2.0, and 5.0 m/

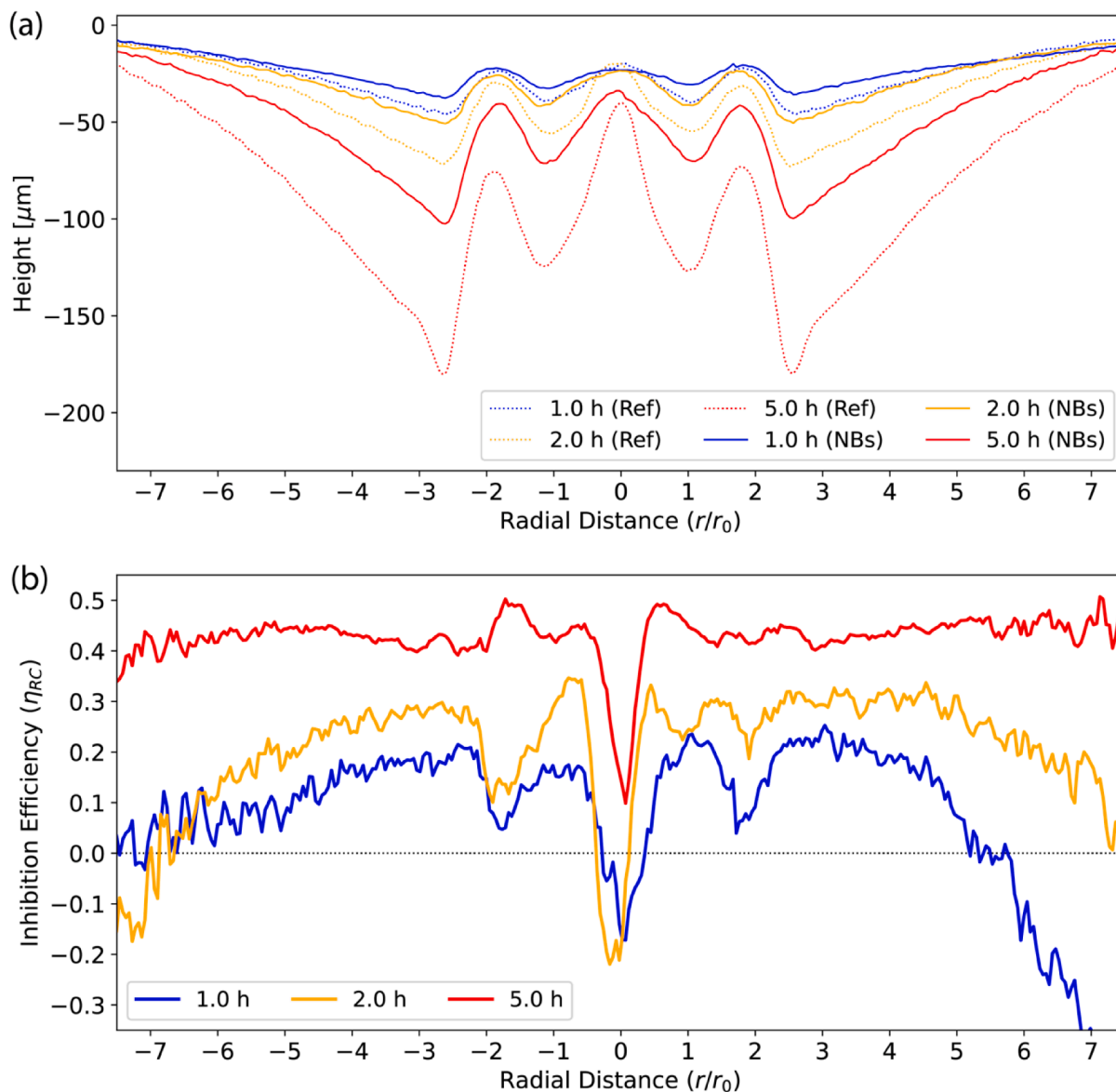


Fig. 9. (a) Surface roughness of the given specimen with the reference CuCl_2 solution ("Ref") and NBs-containing CuCl_2 solution ("NBs") after jet impingement test for 1.0, 2.0, and 5.0 h with a jet exit velocity of 5.0 m/s. The accuracy of measured height is $\pm 3 \mu\text{m}$. (b) Inhibition efficiency $\eta_{RC}(r, t)$ at 1.0, 2.0, and 5.0 h of jet impingement test with a jet exit velocity of 5.0 m/s.

s (Fig. 11). The obtained relationship is valid for the NBs-containing solution because the chemical and hydrodynamical properties of specimen material and fluid flow, which can change the constants a and b , are assumed to be identical in our experiment. From our results at 5.0 h and $r/r_0 = 3.0$ (Fig. 9a), the corrosion rates of the specimen R_{corr} in the NBs-containing fluid are calculated as $97.1 \pm 5.3 \text{ mm/yr}$ and $157.7 \pm 5.3 \text{ mm/yr}$ with jet exit velocities of 2.0 m/s and 5.0 m/s, respectively. This results that the wall shear stresses τ_w in the NBs-containing fluid are respectively $6.0(\pm 0.8) \text{ Pa}$ and $20.2(+1.7/-1.6) \text{ Pa}$ with jet exit velocities of 2.0 m/s and 5.0 m/s from the obtained relationship (Fig. 11), accounting for significant reductions in the wall shear stress in the highly turbulent region of $58(+5/-6)\%$ and $73(\pm 2)\%$, respectively. We thus suggest that NBs mitigate flow-accelerated copper corrosion by playing a role in reducing wall shear stress and that the reduction by NBs is more significant with a higher jet exit velocity. We presume that surface NBs, with a height of a few tens of nm pinned to the copper surface, contribute more to the significant reduction in wall shear stress by generating a bubble mattress at the interface between liquid and copper than bulk NBs. Surface NBs enable the reduction of wall shear

stress in a turbulent flow, likely by the large slip at the liquid-solid interface; however, further studies are necessary to understand the concrete mechanism of wall shear stress reduction and corrosion inhibition.

We cannot conclude whether the size of NBs varies the inhibition efficiency of flow-accelerated corrosion. On the other hand, we presume that the inhibition efficiency can be greater with higher number densities of NBs. The number densities of NBs generated by commercial and in-house NB generators are on the order of magnitudes from 10^6 to 10^{11} bubbles/mL and are typically $\sim 10^8$ bubbles/mL [29,31,53]. The NB generator we used in this study generates NBs with a number density of $\sim 6 \times 10^7$ bubbles/mL, which is slightly lower than the typical number density of NBs previously reported. This fact emphasizes our results that such a relatively low number density of NBs can demonstrate a significant reduction in the wall shear stress on the metal surface in turbulent flow regimes and inhibit flow-accelerated corrosion. Therefore, our results suggest that the inhibition effectiveness can be greater with a higher number density of NBs because the coverage fraction of NBs on the metal surface increases if surface NBs play a profound role in

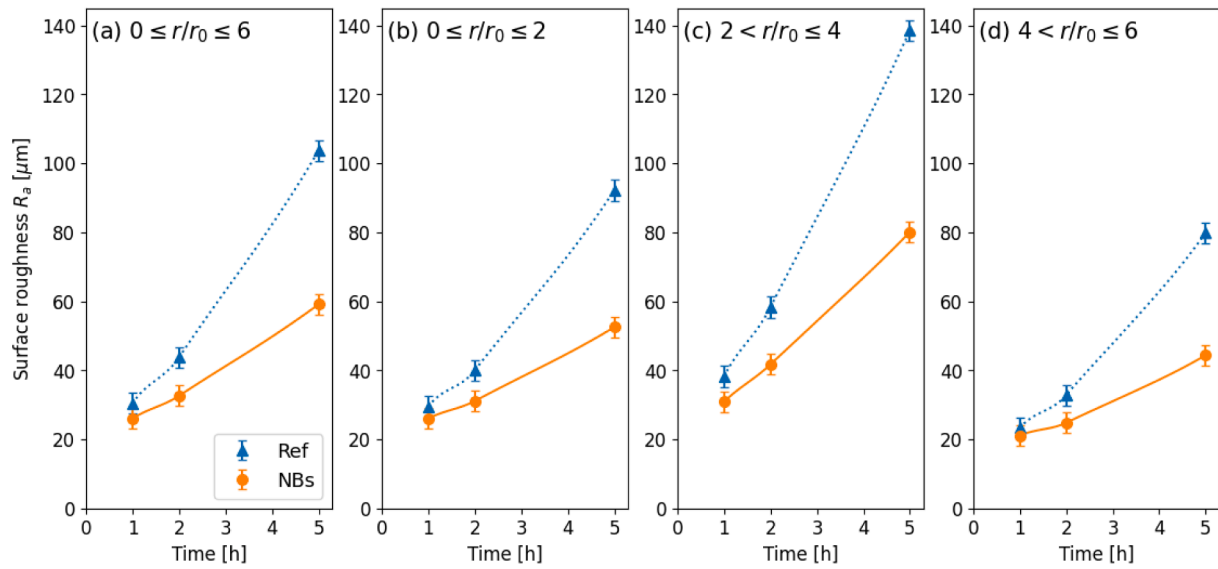


Fig. 10. Arithmetic average roughness R_a of the given specimen with the reference CuCl_2 solution (“Ref”) and NBs-containing CuCl_2 solution (“NBs”) after jet impingement test for 1.0, 2.0, and 5.0 h with a jet exit velocity of 5.0 m/s. (a) Arithmetic average roughness R_a at the radial distance of $0 \leq r/r_0 \leq 6$. (b) Arithmetic average roughness R_a at the radial distance of $0 \leq r/r_0 \leq 2$. (c) Arithmetic average surface roughness R_a at the radial distance of $2 < r/r_0 \leq 4$. (d) Arithmetic average roughness R_a at the radial distance of $4 < r/r_0 \leq 6$.

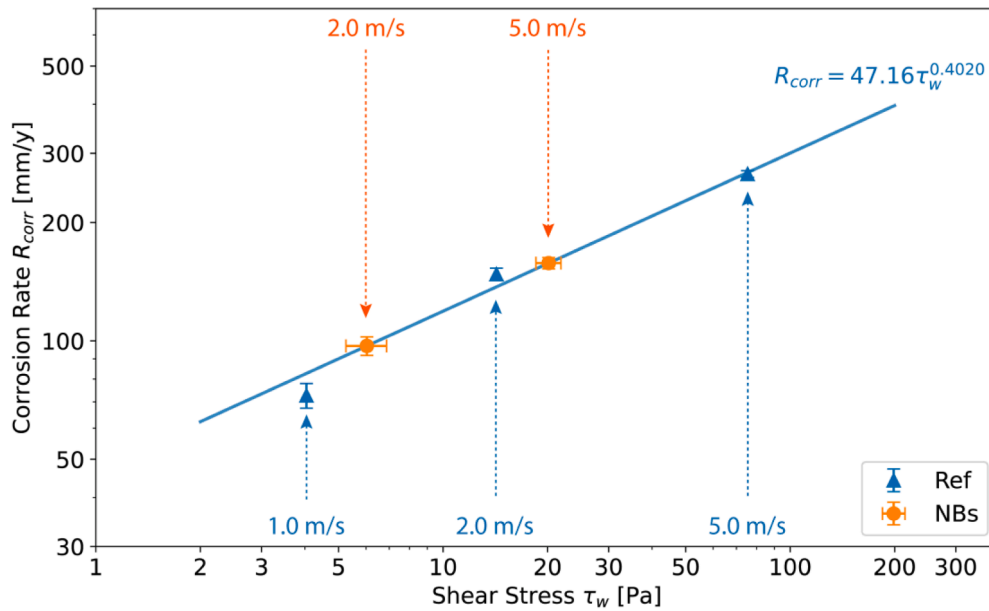


Fig. 11. Corrosion rate R_{corr} (mm/yr) in the reference CuCl_2 solution as a function of wall shear stress τ_w (Pa). The solid line shows the obtained power law relationship.

corrosion mitigation. Verifying the hypothesis and better understanding the inhibition mechanism by NBs will be the future studies using electrochemical methods [62].

5. Conclusions

This paper studied the use of nanobubbles (NBs) or ultrafine bubbles as an inhibitor of flow-accelerated corrosion under the impingement of a turbulent liquid jet. We examined the corrosion inhibition efficiency of copper specimens for 5 h in the flow regime at a Reynolds number Re of from 6.1×10^3 to 3.0×10^4 , with adding $6.0(\pm 0.4) \times 10^7$ bubbles/mL of air-NBs (median diameter: 75 ± 5 nm) to the tested liquid of 0.25% CuCl_2 solution at 40 °C. We measured weight losses, analyzed microstructure

using SEM, and acquired the maximum erosion depth and roughness curve of tested copper specimens. We found that NBs mitigated the flow-accelerated copper corrosion under the jet impingement, despite our experiment being done in highly erosive/corrosive and turbulent conditions. The inhibition efficiencies of flow-accelerated corrosion based on weight loss and maximum erosion depth were up to $43.9 \pm 0.1\%$ and $69.5 \pm 1.8\%$, respectively. The inhibition efficiency generally increased with a higher jet outlet velocity and longer test time of jet impingement. The inhibition is likely due to the significant reduction of wall shear stress on the copper surface in the highly turbulent region due to surface NBs pinned on the copper surface, resulting in up to $73 \pm 2\%$ reduction in the tested time of jet impingement. Our findings suggest that NBs can be a low-cost, environmentally benign, and highly effective nanostructured

material for inhibiting corrosion in hydrodynamically very erosive/corrosive conditions where most inhibitors could not work well.

CRediT authorship contribution statement

Naruhito Katagiri: Conceptualization, Data curation, Formal analysis, Investigation, Methodology, Project administration, Resources, Validation, Visualization, Writing – review & editing. **Arata Kioka:** Data curation, Formal analysis, Investigation, Methodology, Validation, Visualization, Writing – original draft. **Masao Nonoyama:** Conceptualization, Project administration, Resources, Writing – review & editing. **Yuichi Hayashi:** Conceptualization, Project administration, Resources, Writing – review & editing.

Declaration of Competing Interest

The authors declare that they have no known competing financial interests or personal relationships that could have appeared to influence the work reported in this paper.

Data availability

Data will be made available upon request.

Acknowledgement

The authors thank N. Yamamoto for assisting the SEM measurement. A.K. was supported by JSPS KAKENHI Grant-in-Aid for Early-Career Scientists (JP21K14576).

References

- [1] A. Fateh, M. Aliofkhaezai, A.R. Rezvanian, Review of corrosive environments for copper and its corrosion inhibitors, *Arab. J. Chem.* 13 (2020) 481–544, <https://doi.org/10.1016/j.arabj.2017.05.021>.
- [2] A.M. Dietrich, D. Glindemann, F. Pizarro, V. Gidi, M. Olivares, M. Araya, A. Camper, S. Duncan, S. Dwyer, A.J. Whelton, T. Younos, S. Subramanian, G. A. Burlingame, D. Khiari, M. Edwards, Health and aesthetic impacts of copper corrosion on drinking water, *Water Sci. Technol.* 49 (2004) 55–62, <https://doi.org/10.2166/wst.2004.0087>.
- [3] Y. Feng, K.S. Siow, W.K. Teo, K.L. Tan, A.K. Hsieh, Corrosion mechanisms and products of copper in aqueous solutions at various pH values, *CORROSION* 53 (1997) 389–398, <https://doi.org/10.5006/1.3280482>.
- [4] Y. Zhao, R. Mirzaei, Investigating the flow induced corrosion of copper in chloride-containing solution at the atomistic scale, *Appl. Surf. Sci.* 538 (2021), 147925, <https://doi.org/10.1016/j.apsusc.2020.147925>.
- [5] H. Otmačić, E. Stupnišek-Lisac, Copper corrosion inhibitors in near neutral media, *Electrochim. Acta* 48 (2003) 985–991, [https://doi.org/10.1016/S0013-4686\(02\)00811-3](https://doi.org/10.1016/S0013-4686(02)00811-3).
- [6] M.M. Antonijević, S.M. Milić, M.B. Petrović, Films formed on copper surface in chloride media in the presence of azoles, *Corros. Sci.* 51 (2009) 1228–1237, <https://doi.org/10.1016/j.corsci.2009.03.026>.
- [7] M. Finšgar, I. Milošev, Inhibition of copper corrosion by 1,2,3-benzotriazole: a review, *Corros. Sci.* 52 (2010) 2737–2749, <https://doi.org/10.1016/j.corsci.2010.05.002>.
- [8] Y. Tan, Y. Fwu, K. Bhardwaj, Electrochemical evaluation of under-deposit corrosion and its inhibition using the wire beam electrode method, *Corros. Sci.* 53 (2011) 1254–1261, <https://doi.org/10.1016/j.corsci.2010.12.015>.
- [9] S. Li, S. Chen, S. Lei, H. Ma, R. Yu, D. Liu, Investigation on some Schiff bases as HCl corrosion inhibitors for copper, *Corros. Sci.* 41 (1999) 1273–1287, [https://doi.org/10.1016/S0010-938X\(98\)00183-8](https://doi.org/10.1016/S0010-938X(98)00183-8).
- [10] H. Ma, S. Chen, L. Niu, S. Zhao, S. Li, D. Li, Inhibition of copper corrosion by several Schiff bases in aerated halide solutions, *J. Appl. Electrochem.* 32 (2002) 65–72, <https://doi.org/10.1023/A:1014242112512>.
- [11] K.M. Ismail, Evaluation of cysteine as environmentally friendly corrosion inhibitor for copper in neutral and acidic chloride solutions, *Electrochim. Acta* 52 (2007) 7811–7819, <https://doi.org/10.1016/j.electacta.2007.02.053>.
- [12] K. Barouni, L. Bazzi, R. Salghi, M. Mihit, B. Hammouti, A. Albourine, S. El Issami, Some amino acids as corrosion inhibitors for copper in nitric acid solution, *Mater. Lett.* 62 (2008) 3325–3327, <https://doi.org/10.1016/j.matlet.2008.02.068>.
- [13] D.Q. Zhang, Q.R. Cai, X.M. He, L.X. Gao, G.S. Kim, Corrosion inhibition and adsorption behavior of methionine on copper in HCl and synergistic effect of zinc ions, *Mater. Chem. Phys.* 114 (2009) 612–617, <https://doi.org/10.1016/j.matchemphys.2008.10.007>.
- [14] K.F. Khaled, Corrosion control of copper in nitric acid solutions using some amino acids – A combined experimental and theoretical study, *Corros. Sci.* 52 (2010) 3225–3234, <https://doi.org/10.1016/j.corsci.2010.05.039>.
- [15] A. Ulman, Formation and structure of self-assembled monolayers, *Chem. Rev.* 96 (1996) 1533–1554, <https://doi.org/10.1021/cr9502357>.
- [16] G.K. Jennings, T.H. Yong, J.C. Munro, P.E. Laibinis, Structural effects on the barrier properties of self-assembled monolayers formed from long-chain ω -alkoxy-n-alkanethiols on copper, *J. Am. Chem. Soc.* 125 (2003) 2950–2957, <https://doi.org/10.1021/ja020233i>.
- [17] A. Fouda, M. El-Haddad, Y. Abdallah, Septazole: antibacterial drug as a green corrosion inhibitor for copper in hydrochloric acid solutions, *Int. J. Innov. Res. Sci. Eng. Technol.* 2 (2013) 7073–7085.
- [18] A. Jmiai, A. Tara, S. El Issami, M. Hilali, O. Jbara, L. Bazzi, A new trend in corrosion protection of copper in acidic medium by using Jujube shell extract as an effective green and environmentally safe corrosion inhibitor: experimental, quantum chemistry approach and Monte Carlo simulation study, *J. Mol. Liq.* 322 (2021), 114509, <https://doi.org/10.1016/j.molliq.2020.114509>.
- [19] B. Evgeny, T. Hughes, D. Eskin, Effect of surface roughness on corrosion behaviour of low carbon steel in inhibited 4M hydrochloric acid under laminar and turbulent flow conditions, *Corros. Sci.* 103 (2016) 196–205, <https://doi.org/10.1016/j.corsci.2015.11.019>.
- [20] E.V. Senatore, W. Taleb, J. Owen, Y. Hua, J.A.C.P. Gomes, R. Barker, A. Neville, Evaluation of high shear inhibitor performance in CO₂-containing flow-induced corrosion and erosion-corrosion environments in the presence and absence of iron carbonate films, *Wear* 404–405 (2018) 143–152, <https://doi.org/10.1016/j.wear.2018.03.014>.
- [21] M. Braut, L. González-Fernández, A. Kosinska, Y. Grosu, P. Kosinski, B.V. Balakin, Experimental investigation of erosion due to nanofluids, *Wear* 502–503 (2022), 204378, <https://doi.org/10.1016/j.wear.2022.204378>.
- [22] L. Chaal, C. Deslouis, A. Pailleret, B. Saidani, On the mitigation of erosion-corrosion of copper by a drag-reducing cationic surfactant in turbulent flow conditions using a rotating cage, *Electrochim. Acta* 52 (2007) 7786–7795, <https://doi.org/10.1016/j.electacta.2006.10.013>.
- [23] M. Lavanya, V.R. Murthy, P. Rao, Performance evaluation of a potent green inhibitor on 6061 aluminum alloy under liquid/solid jet impingement, *J. Bio-Tribo-Corrosion*. 5 (2019) 93, <https://doi.org/10.1007/s40735-019-0288-7>.
- [24] M. Lavanya, V.R. Murthy, P. Rao, Erosion corrosion control of 6061 aluminum alloy in multi-phase jet impingement conditions with eco-friendly green inhibitor, *Chinese J. Chem. Eng.* 28 (2020) 340–347, <https://doi.org/10.1016/j.cjche.2019.07.016>.
- [25] J.W.G. Tyrrell, P. Attard, Images of nanobubbles on hydrophobic surfaces and their interactions, *Phys. Rev. Lett.* 87 (2001), 176104, <https://doi.org/10.1103/PhysRevLett.87.176104>.
- [26] M. Switkes, J.W. Ruberti, Rapid cryofixation/freeze fracture for the study of nanobubbles at solid-liquid interfaces, *Appl. Phys. Lett.* 84 (2004) 4759–4761, <https://doi.org/10.1063/1.1755837>.
- [27] A. Agrawal, J. Park, D.Y. Ryu, P.T. Hammond, T.P. Russell, G.H. McKinley, Controlling the location and spatial extent of nanobubbles using hydrophobically nanopatterned surfaces, *Nano Lett.* 5 (2005) 1751–1756, <https://doi.org/10.1021/nl051103o>.
- [28] D. Lohse, X. Zhang, Surface nanobubbles and nanodroplets, *Rev. Mod. Phys.* 87 (2015) 981–1035, <https://doi.org/10.1103/RevModPhys.87.981>.
- [29] M. Alheshibri, J. Qian, M. Jehannin, V.S.J. Craig, A history of nanobubbles, *Langmuir* 32 (2016) 11086–11100, <https://doi.org/10.1021/acs.langmuir.6b02489>.
- [30] T. Temesgen, T.T. Bui, M. Han, T. Kim, H. Park, Micro and nanobubble technologies as a new horizon for water-treatment techniques: a review, *Adv. Colloid Interface Sci.* 246 (2017) 40–51, <https://doi.org/10.1016/j.cis.2017.06.011>.
- [31] A.J. Atkinson, O.G. Apul, O. Schneider, S. Garcia-Segura, P. Westerhoff, Nanobubble technologies offer opportunities to improve water treatment, *Acc. Chem. Res.* 52 (2019) 1196–1205, <https://doi.org/10.1021/acs.accounts.8b00606>.
- [32] N. Nirmalkar, A.W. Pacek, M. Barigou, On the existence and stability of bulk nanobubbles, *Langmuir* 34 (2018) 10964–10973, <https://doi.org/10.1021/acs.langmuir.8b01163>.
- [33] K. Yasui, T. Tuziuti, W. Kanematsu, Mysteries of bulk nanobubbles (ultrafine bubbles); stability and radical formation, *Ultrason. Sonochem.* 48 (2018) 259–266, <https://doi.org/10.1016/j.ultrsonch.2018.05.038>.
- [34] E.D. Michailidi, G. Bomis, A. Varoutoglou, G.Z. Kyzas, G. Mitrikas, A. C. Mitropoulos, E.K. Efthimiadou, E.P. Favvas, Bulk nanobubbles: production and investigation of their formation/stability mechanism, *J. Colloid Interface Sci.* 564 (2020) 371–380, <https://doi.org/10.1016/j.jcis.2019.12.093>.
- [35] X. Zhang, H. Lhuissier, C. Sun, D. Lohse, Surface nanobubbles nucleate microdroplets, *Phys. Rev. Lett.* 112 (2014), 144503, <https://doi.org/10.1103/PhysRevLett.112.144503>.
- [36] M. Li, X. Ma, J. Eisener, P. Pfeiffer, C.D. Ohl, C. Sun, How bulk nanobubbles are stable over a wide range of temperatures, *J. Colloid Interface Sci.* 596 (2021) 184–198, <https://doi.org/10.1016/j.jcis.2021.03.064>.
- [37] Y.W. Fan, R.Z. Wang, Submicrometer-sized vaterite tubes formed through nanobubble-templated crystal growth, *Adv. Mater.* 17 (2005) 2384–2388, <https://doi.org/10.1002/adma.200500755>.
- [38] K. Tagomori, A. Kioka, M. Nakagawa, A. Ueda, K. Sato, K. Yonezu, S. Anzai, Air nanobubbles retard calcite crystal growth, *Colloids Surf. A Physicochem. Eng. Asp.* 648 (2022), 129319, <https://doi.org/10.1016/j.colsurfa.2022.129319>.

- [39] I.D. Tegladza, G. Lin, C. Liu, X. Gu, Control of crystal nucleation, size and morphology using micro-/nanobubbles as green additives – a review, *Sep. Purif. Technol.* 311 (2023), 123232, <https://doi.org/10.1016/j.seppur.2023.123232>.
- [40] Y. Zhang, H. Duan, E. Chen, M. Li, S. Liu, Physicochemical characteristics and the scale inhibition effect of air nanobubbles (A-NBs) in a circulating cooling water system, *Langmuir* 39 (2023) 1629–1639, <https://doi.org/10.1021/acs.langmuir.2c03075>.
- [41] Y. Xie, C. Zhao, An optothermally generated surface bubble and its applications, *Nanoscale* 9 (2017) 6622–6631, <https://doi.org/10.1039/C7NR01360D>.
- [42] R. Xiong, D. Hua, J. Van Hoeck, D. Berdecka, L. Léger, S. De Munter, J.C. Fraire, L. Raes, A. Harizaj, F. Sauvage, G. Goetgeluk, M. Pille, J. Aalders, J. Belza, T. Van Acker, E. Bolea-Fernandez, T. Si, F. Vanhaecke, W.H. De Vos, B. Vandekerckhove, J. van Hengel, K. Raemdonck, C. Huang, S.C. De Smedt, K. Braeckmans, Photothermal nanofibres enable safe engineering of therapeutic cells, *Nat. Nanotechnol.* 16 (2021) 1281–1291, <https://doi.org/10.1038/s41565-021-00976-3>.
- [43] M. Alheshibri, A. Al Baroot, L. Shui, M. Zhang, Nanobubbles and nanoparticles, *Curr. Opin. Colloid Interface Sci.* 55 (2021), 101470, <https://doi.org/10.1016/j.cocis.2021.101470>.
- [44] E.Y. Lukianova-Hleb, X. Ren, J.A. Zasadzinski, X. Wu, D.O. Lapotko, Plasmonic nanobubbles enhance efficacy and selectivity of chemotherapy against drug-resistant cancer cells, *Adv. Mater.* 24 (2012) 3831–3837, <https://doi.org/10.1002/adma.201103550>.
- [45] R. Xiong, R.X. Xu, C. Huang, S. De Smedt, K. Braeckmans, Stimuli-responsive nanobubbles for biomedical applications, *Chem. Soc. Rev.* 50 (2021) 5746–5776, <https://doi.org/10.1039/C9CS00839J>.
- [46] M. Ito, Y. Sugai, Nanobubbles activate anaerobic growth and metabolism of *Pseudomonas aeruginosa*, *Sci. Rep.* 11 (2021) 16858, <https://doi.org/10.1038/s41598-021-96503-4>.
- [47] P. Pal, H. Anantharaman, CO₂ nanobubbles utility for enhanced plant growth and productivity: recent advances in agriculture, *J. CO₂ Util.* 61 (2022), 102008, <https://doi.org/10.1016/j.jcou.2022.102008>.
- [48] K.K.T. Phan, T. Truong, Y. Wang, B. Bhandari, Nanobubbles: fundamental characteristics and applications in food processing, *Trends Food Sci. Tech.* 95 (2020) 118–130, <https://doi.org/10.1016/j.tifs.2019.11.019>.
- [49] M. FAN, D. TAO, R. HONAKER, Z. LUO, Nanobubble generation and its applications in froth flotation (part III): specially designed laboratory scale column flotation of phosphate, *Min. Sci. Technol.* 20 (2010) 317–338, [https://doi.org/10.1016/S1674-5264\(09\)60205-2](https://doi.org/10.1016/S1674-5264(09)60205-2).
- [50] A. Azevedo, R. Etchepare, S. Calgaroto, J. Rubio, Aqueous dispersions of nanobubbles: generation, properties and features, *Miner. Eng.* 94 (2016) 29–37, <https://doi.org/10.1016/j.mineng.2016.05.001>.
- [51] V. Chipakwe, R. Jolsterå, S.C. Chelgani, Nanobubble-assisted flotation of apatite tailings: insights on beneficiation options, *ACS Omega* 6 (2021) 13888–13894, <https://doi.org/10.1021/acsomega.1c01551>.
- [52] A. Aikawa, A. Kioka, M. Nakagawa, S. Anzai, Nanobubbles as corrosion inhibitor in acidic geothermal fluid, *Geothermics* 89 (2021), 101962, <https://doi.org/10.1016/j.geothermics.2020.101962>.
- [53] A. Kioka, M. Nakagawa, Theoretical and experimental perspectives in utilizing nanobubbles as inhibitors of corrosion and scale in geothermal power plant, *Renew. Sustain. Energy Rev.* 149 (2021), 111373, <https://doi.org/10.1016/j.rser.2021.111373>.
- [54] B. Poulson, Electrochemical measurements in flowing solutions, *Corros. Sci.* 23 (1983) 391–430, [https://doi.org/10.1016/0010-938X\(83\)90070-7](https://doi.org/10.1016/0010-938X(83)90070-7).
- [55] F. Giralt, O. Trass, Mass transfer from crystalline surfaces in a turbulent impinging jet part I. Transfer by erosion, *Can. J. Chem. Eng.* 53 (1975) 505–511, <https://doi.org/10.1002/cjce.5450530508>.
- [56] K.D. Eifird, E.J. Wright, J.A. Boros, T.G. Hailey, Correlation of steel corrosion in pipe flow with jet impingement and rotating cylinder tests, *CORROSION* 49 (1993) 992–1003, <https://doi.org/10.5006/1.3316026>.
- [57] D.J. Phares, G.T. Smedley, R.C. Flagan, The wall shear stress produced by the normal impingement of a jet on a flat surface, *J. Fluid Mech.* 418 (2000) 351–375, <https://doi.org/10.1017/S002211200000121X>.
- [58] M. Nakagawa, A. Kioka, K. Tagomori, Nanobubbles as friction modifier, *Tribol. Int.* 165 (2022), 107333, <https://doi.org/10.1016/j.triboint.2021.107333>.
- [59] C. Vega-Sánchez, S. Peppou-Chapman, L. Zhu, C. Neto, Nanobubbles explain the large slip observed on lubricant-infused surfaces, *Nat. Commun.* 13 (2022) 351, <https://doi.org/10.1038/s41467-022-28016-1>.
- [60] A. Demoz, T. Dabros, Relationship between shear stress on the walls of a pipe and an impinging jet, *Corros. Sci.* 50 (2008) 3241–3246, <https://doi.org/10.1016/j.corsci.2008.08.025>.
- [61] M. Metikoš-Huković, R. Babić, I. Škugor Rončević, Z. Grubač, Corrosion behavior of the filmed copper surface in saline water under static and jet impingement conditions, *CORROSION* 68 (2012), 025002–1–025002–8, <https://doi.org/10.5006/1.3683224>.
- [62] F. Farelles, M. Galicia, B. Brown, S. Nesic, H. Castaneda, Evolution of dissolution processes at the interface of carbon steel corroding in a CO₂ environment studied by EIS, *Corros. Sci.* 52 (2010) 509–517, <https://doi.org/10.1016/j.corsci.2009.10.007>.